



Cosmogenic ${}^3\text{He}$ in hematite and goethite from Brazilian “canga” duricrust demonstrates the extreme stability of these surfaces

David L. Shuster ^{a,b,*}, Kenneth A. Farley ^c, Paulo M. Vasconcelos ^d, Greg Balco ^b, Hevelyn S. Monteiro ^d, Kathryn Waltenberg ^d, John O. Stone ^e

^a Department of Earth and Planetary Science, University of California, Berkeley, CA 94720, USA

^b Berkeley Geochronology Center, 2455 Ridge Road, Berkeley, CA 94709, USA

^c Division of Geological and Planetary Sciences, California Institute of Technology, Pasadena, CA 91125, USA

^d Department of Earth Sciences, University of Queensland, Brisbane, Queensland 4072, Australia

^e Department of Earth and Space Sciences, University of Washington, Seattle, WA 98195, USA

ARTICLE INFO

Article history:

Received 1 November 2011

Received in revised form 9 February 2012

Accepted 17 February 2012

Available online xxxx

Editor: B. Marty

Keywords:

cosmogenic nuclide geochronology

${}^3\text{He}$

${}^{21}\text{Ne}$

laterite

chemical weathering

production rate calibration

ABSTRACT

Helium isotopes were measured in hematite and goethite samples from several lateritic duricrusts (canga) developed on banded iron formations. These samples uniformly have high ${}^3\text{He}$ concentrations which must arise from long periods of cosmic ray exposure. From coexisting phases from the Quadrilátero Ferrífero in east central Brazil, we determined the ratio of cosmogenic ${}^3\text{He}$ in hematite to that of ${}^{21}\text{Ne}$ in quartz to be 3.96 ± 0.19 . Combined with best current estimates of the ${}^{21}\text{Ne}$ production rate in quartz, this ratio implies a sea-level high latitude (SLHL) ${}^3\text{He}$ production rate in hematite of 68.1 ± 8.1 atoms/g/yr; from the chemical composition we estimate the ${}^3\text{He}$ production rate in goethite to be ~5% higher. We use these production rate estimates to interpret ${}^3\text{He}$ concentrations measured in goethite and hematite from a ~10 m depth profile collected from a surface canga in Carajás, in the Amazon basin of Brazil. We find that the Carajás canga has experienced a very low rate of surface erosion (~0.16–0.54 m/Myr) over at least the last few millions of years. This iron-rich canga surface is remarkably resistant to erosion despite its location in a wet tropical environment. Details of the depth profile suggest that despite its stability, the canga has also been internally dynamic (translocation of material; solution and reprecipitation) over million-year timescales.

© 2012 Published by Elsevier B.V.

1. Introduction

One result of pervasive chemical weathering of rock exposed near earth's surface is removal of soluble elements from the original lithology, and precipitation of more thermodynamically-stable oxides [e.g., (Anderson et al., 2002; Brimhall et al., 1991; Meybeck, 1987)]. When the primary lithology is iron-rich, such as a banded iron formation [BIF; (James, 1983)], and when in a tectonically stable setting, massive quantities of secondary iron oxides and oxyhydroxides (hereafter Fe-oxides) can precipitate near the surface. These resulting deposits of mostly goethite (FeOOH) and hematite (Fe_2O_3) can form a chemically stable surface, which is termed “canga”, ferricrete, or ferruginous duricrust (Dorr, 1964; Harder and Chamberlin, 1915; Mabesoone, 1965; Samama, 1986). Because these massive crusts of iron oxides are physically strong and chemically stable, they are relatively resistant to erosion such that in some landscapes they define high standing plateaus (Dorr, 1964; Klein and Ladeira, 2002; Spier et al., 2007;

Vasconcelos et al., 1994a), particularly when the landscape is transport-limited (Carson and Kirkby, 1972).

Chemical reactions associated with deep lateritization are complex and can occur episodically and over very long periods of time (Vasconcelos, 1999). The net effect of these reactions is to remove soluble species from chemically reactive rock to produce an insoluble residue that is typically rich in iron and aluminum (Brimhall et al., 1991). This enrichment process is of great significance in producing some of the largest high-purity iron deposits on Earth. The processes that result in canga formation involve partial dissolution of primary minerals in the BIFs (e.g., carbonates, quartz, hematite, and magnetite), collapse and recementation of partially leached BIF fragments, and the precipitation of multiple generations of supergene Fe-oxides at various points in time and depth beneath the evolving surface. The near-surface precipitation of Fe-oxides from solution can occur simultaneously with the downward propagation of a chemical weathering front – possibly at significant depths beneath the canga – while increasing permeability into un-weathered bedrock (Brimhall et al., 1991; Klein and Ladeira, 2002; Ramanaidou, 2009; Vasconcelos, 1999).

Geochronological methods applied to minerals that precipitate in the weathering environment constrain the timing of specific chemical reactions, and hence physical and chemical conditions, leading to their

* Corresponding author at: Berkeley Geochronology Center, 2455 Ridge Road, Berkeley, CA 94709, USA. Tel.: +1 510 644 9200; fax: +1 510 644 9201.

E-mail address: dshuster@berkeley.edu (D.L. Shuster).

precipitation (Vasconcelos et al., 1992; Yapp and Shuster, 2011). For example, the $^{40}\text{Ar}/^{39}\text{Ar}$ method applied to manganese oxides and sulfates from Brazil (Vasconcelos et al., 1994b), Africa (Vasconcelos et al., 1994a), China (Li et al., 2007) and Australia (Li and Vasconcelos, 2002; Vasconcelos and Conroy, 2003) and the (U-Th)/He system applied to iron oxides from Brazil (Shuster et al., 2005) and Australia (Heim et al., 2006) have shown that the precipitation of these phases in deeply weathered environments has been episodic and that some have existed throughout at least the Cenozoic (Vasconcelos, 1999; Vasconcelos et al., 2008).

Despite their stability, lateritic profiles are chemically and physically dynamic. For example, cosmogenic nuclides have been used to quantify rates of surface erosion and have revealed changes in depths and relative positions of clasts due to bio-pedoturbation during profile development [e.g., (Braucher et al., 2000; Brown et al., 1994)]. These studies analyzed quartz so could only be applied to profiles containing significant quantities of quartz in the regolith. The more geomorphically notable and economically important canga deposits tend to contain little quartz, thus motivating our interest in cosmogenic ^3He production in Fe-oxides. Furthermore, the geo-chemical and -morphological processes that occur in the lateritic profile and that result in high-standing topography composed primarily of deeply weathered rocks, and their persistence under wet, tropical conditions remain poorly understood.

The objective of the present study is to develop a geochronological tool for studying the long-term development and stability of Fe-oxides produced by chemical weathering near the rock-atmosphere interface. In this work, we estimate the production rate of cosmogenic ^3He in hematite and goethite from cosmogenic ^{21}Ne in coexisting quartz. To our knowledge the production rate has not previously been established for either of these phases. We then use observations of ^3He in the iron oxides to quantify the surface erosion rate of a ferricrete duricrust in the Brazilian Amazon.

2. Field sites

2.1. Production rate calibration site selection—Quadrilátero Ferrífero, Brazil

Although the production rate of cosmogenic nuclides in a mineral of a given composition can be estimated from element-specific nuclear reaction rates and the cosmic-ray flux (Masarik, 2002; Masarik and Reedy, 1995), the uncertainty on these estimates is potentially large. As a result production rates are most often determined empirically. Because cosmogenic ^3He production rates will vary only slightly between nearby elements in the periodic table, it is reasonable to expect that the ^3He production rate in hematite (Fe_2O_3) and goethite (FeOOH) will be similar to the production rates in other iron and titanium bearing oxides such as magnetite and ilmenite. The most detailed empirical work on such phases was done by Kober et al. (2005), who compared cosmogenic ^3He concentrations in FeTi oxides to ^{21}Ne in coexisting quartz from the Chilean Andes. Based on the $^3\text{He}/^{21}\text{Ne}$ ratios and an assumed ^{21}Ne production rate in quartz of 20.3 atom/g/yr, these authors estimated an SLHL ^3He production rate in FeTi oxides of 120 ± 11 atom/g/yr, a value they assert is consistent with their reassessment of nuclear cross section data. In contrast, limited empirical studies by others suggest far lower production rates of about 70 atom/g/yr for magnetite and ilmenite (Bryce and Farley, 2002; Margerison et al., 2005). The origin of this extremely large discrepancy is unclear. This discrepancy in apparent rate of ^3He production from Fe is an important motivation for the present work.

For this part of our study our objective was to identify a field site in which hematite coexists with quartz at earth's surface. Production rates of cosmogenic ^{10}Be , ^{26}Al and ^{21}Ne production in quartz are independently known (Dunai, 2010). Thus, measuring the ratio of ^3He

in hematite to one or more of these nuclides in coexisting quartz provides an estimate of the ^3He production rate.

During the formation of cangas, most of the fine-grained quartz present in the BIF (particularly jaspilitic BIFs) is leached away. Fine-grained hematite and magnetite are also dissolved or hydrated into supergene goethite. However, BIFs at the Quadrilátero Ferrífero, Minas Gerais, Brazil, have undergone amphibolite grade metamorphism, resulting in coarse-grained hematite, magnetite, and quartz in a rock commonly known as itabirite. Quartz and hematite in itabirites can be very coarse grained (several centimeters), and some of these primary phases partially survive the reactions leading to cangas. Primary quartz and hematite in this lithology are suitable for our purposes because both minerals formed well before exposure to surface cosmic rays, and experienced identical exposure histories thereafter.

We sampled such coarse-grained vein quartz and coexisting hematite from the Pico Iron Mine (20.1498 S and 43.8762 W, 1560 m elevation). The sample PIC-06-12 was collected from the upper 5 cm surface of the canga horizon, which was produced by deep lateritization of the underlying BIF (Spier et al., 2007). Quartz in this sample, analyzed using standard methods [see (Stone, 2004) and (Rood et al., 2010)], has 7.496 ± 0.080 Matoms/g cosmogenic ^{10}Be and 42.4 ± 1.0 Matoms/g cosmogenic ^{26}Al implying simple exposure (Lal, 1991) with an apparent exposure age of 1.4 Ma or steady erosion rate of $100 \text{ g/cm}^2/\text{Ma}$ (0.37 m/Ma for 2.7 g/cm^3 density)—an extremely low erosion rate. The relationship between stable ^3He and radioactive ^{10}Be and ^{26}Al is strongly dependent on the details of such a long duration exposure, which are not independently known for this sample. Thus, we cannot accurately estimate the ^3He production rate from these ^{10}Be and ^{26}Al results.

Therefore, we determined the ratio of ^3He in hematite to ^{21}Ne in quartz, and calculate the ^3He production rate by reference to the known ^{21}Ne production rate in quartz (Balco and Shuster, 2009). This procedure does not require that the exposure history be known; it only requires that both hematite and quartz share common exposure history (as indicated by field relationships and the petrography of our sample) and that both nuclides are quantitatively retained. If we assume that the production ratio $P^3\text{He}_{\text{hematite}}/P^{21}\text{Ne}_{\text{quartz}}$ does not vary during exposure, then the concentration ratio is also equal to the instantaneous production ratio at any time. This assumption is satisfied if (i) the sample was derived from a surface that was not eroding, or (ii) the production ratio does not vary with depth below the surface, which in turn implies that the production ratio is similar for both high energy neutron spallation and muon interactions. High nuclide concentrations indicating a surface with an extremely low erosion rate suggests this assumption is likely valid due to (i) above. Below, we discuss the possibility that production of ^3He in iron oxides by muons is significantly larger than for ^{21}Ne in quartz; if this were true, this assumption would cause us to overestimate the surface production rate for ^3He in hematite.

2.2. Duricrust depth profile—Carajás, Brazil

To interrogate the stability of an Fe-rich duricrust surface, we collected samples from the uppermost ~10 vertical meters of canga exposed in a wall within an open pit mine of the N4C deposit (6.0299 S, 50.2869 W, 720 m elevation) of Carajás in Pará, Brazil. Like the canga from the Quadrilátero Ferrífero, this canga also resulted from deep lateritization of an underlying BIF (Klein and Ladeira, 2002), leading to an iron-rich duricrust. The canga also contains detrital fragments of partially leached BIF and rubble of previously formed canga bound together by multiple generations of oxyhydroxide cements (mostly goethite and minor gibbsite). Pure goethite cement is dark brown to black and composed of nearly 100% vitreous goethite with minor supergene hematite. A more ochreous and porous cement often contains various proportions of goethite, hematite, and gibbsite. In some locations the canga approaches 20 m in thickness (Beisiegel,

1982). We collected whole-rock samples of the ferruginous duricrust containing both vitreous and ochreous cements. We also obtained hematite samples from two drill cores from 80 to 130 m depth to determine the background ${}^3\text{He}$ in samples shielded from cosmic-rays.

3. Methods

3.1. Sample preparation

Given field and petrographic evidence that our canga samples were composed of various generations of supergene goethite of various ages, and knowing that the age of these goethite cements might vary from several tens of millions of years to a few hundred thousand years (Vasconcelos, 2008), we targeted only hypogene hematite fragments for cosmogenic ${}^3\text{He}$ studies. For our production rate calibration, we extracted fragments of coexisting re-crystallized hematite and quartz from a particularly coarse-grained fragment of Itabirite from the Pico site. Inspection by optical microscopy indicates that the sample may contain more than one generation of metamorphic (or hydrothermal) hematite, however the hematite and quartz clearly precipitated prior to onset of chemical weathering, and therefore shared the same surface exposure. Sub-aliquots of hypogene hematite were hand-picked after crushing. We prepared quartz separates by crushing to a grain size smaller than the original mineral grains, heavy liquid separation, and repeated etching in dilute HF (Kohl and Nishiizumi, 1992); under normal circumstances this procedure results in 15–20% dissolution, which adequately removes grain boundary areas possibly enriched in nucleogenic ${}^{21}\text{Ne}$.

Sample selection from the Carajás profile was more complex because the jaspilites do not survive the weathering processes leading to canas. The chalcedonic silica is completely dissolved, and only small clusters of hematite survive the weathering process. Since jaspilites do not contain coarse-grained hypogene hematite, we had to sample grains of supergene goethite and supergene hematite for our cosmogenic isotope measurements. From each sample in the Carajás depth profile, we separated ~20 mg aliquots of either goethite or hematite for ${}^3\text{He}$ analysis. Pure grains were identified by inspection using optical microscopy, and goethite and hematite grains differentiated by color and luster. Equivalent aliquots of the grains selected for ${}^3\text{He}$ measurements were mounted in acrylic blocks, polished, and analyzed by optical microscopy and scanning electron microscopy to ascertain that the grains were indeed composed of pure goethite or hematite. The identification of some grains was also verified by synchrotron XRD analysis. Because we could not isolate pure aliquots of each phase for all samples, we do not report results from all depths. In the Carajás canga, all of the goethite is unambiguously supergene. Although every effort was made to collect pure goethite from a single generation, petrographic investigation reveals that some of the analyzed fragments may contain multiple generations; they may also contain small amounts of hematite. Likewise, the hematite aliquots may contain multiple generations of supergene precipitates and possibly fragments of primary hematite. We separated much smaller aliquots (~10–100 μg) of goethite for (U-Th)/He analysis. For these smaller aliquots, we could more easily isolate individual generations of goethite; however such samples were more likely to be later overgrowths, which may be inadvertently biased to younger generations.

3.2. Helium isotope measurements in hematite and goethite

Aliquots of hematite or goethite ranging from ~4 to 26 mg were placed within Pt–Ir alloy packets and degassed at 1500 °C (hematite) or 1000 °C (goethite), under static vacuum using a 70 W diode laser (Balco and Shuster, 2009; Shuster et al., 2010). After heating, the extracted volatiles were reacted with a SAES getter and nonreactive volatiles condensed onto a temperature-controlled cryogenic trap held at 11 K. Helium was released from the trap at 33 K and analyzed

using the MAP-215 mass spectrometer in the BGC Noble Gas Thermo-chronometry Lab. The ${}^3\text{He}$ abundance and ${}^3\text{He}/{}^4\text{He}$ ratio were measured using pulse-counting (${}^3\text{He}$) and Faraday cup (${}^4\text{He}$) sector-field mass spectrometry calibrated against reference gas standards and corrected for blank contributions to ${}^3\text{He}$ and ${}^4\text{He}$ (uncertainties in blank corrections are propagated into reported uncertainties; blank corrections were <1%). Abundances were quantified by peak height comparison to aliquots of a manometrically-calibrated He standard with known abundance and ${}^3\text{He}/{}^4\text{He} = 6.09 \times 10^{-4}$. The ${}^3\text{He}$ sensitivity (typically $\sim 1.6 \times 10^5$ atom/Hz) was constant within the measurement range of our analyses, verified by analyzing differently-sized aliquots of the He standard. We observed blank-level abundances (~0.03 and ~10 Matom for ${}^3\text{He}$ and ${}^4\text{He}$, respectively) when reheating each sample to the maximum heating temperature, indicating that all ${}^3\text{He}$ and ${}^4\text{He}$ was extracted.

3.3. Neon isotope measurements in quartz

Four aliquots of quartz from sample PIC-06-12 ranging from ~74 to 135 mg were placed within Ta packets and heated under vacuum using a 150 W diode laser and a similar pyrometer system as described above. To avoid collateral heating of adjacent samples, we used a step-heating procedure in which we completed one heating step for all samples in the chamber before moving to a higher-temperature step.

After heating, the extracted volatiles were processed as above and Ne was purified and separated from other gasses on a temperature-controlled cryogenic trap held at 70 K. The purified Ne was analyzed using the MAP-215 mass spectrometer in the BGC lab. Interferences on ${}^{20}\text{Ne}$ and ${}^{22}\text{Ne}$ from ${}^{40}\text{Ar}^{++}$ and CO_2^{+} , respectively, were corrected for by analyzing the ${}^{39}\text{Ar}^{++}/{}^{39}\text{Ar}^+$ ratio of a spike of ${}^{39}\text{Ar}$ during the analysis of Ne [for full details see (Balco and Shuster, 2009)]. Total amounts of ${}^{20}\text{Ne}$ and ${}^{21}\text{Ne}$ were quantified by peak height comparison to an air standard. Measurements of the air standard yielded Ne isotope ratios indistinguishable from atmospheric values. The Ne sensitivity was verified to be constant within the measurement range of our analyses by varying the volume of the air standards.

All the analyzed quartz samples yielded Ne isotope ratios indistinguishable from the cosmogenic-atmospheric mixing line [e.g., (Niedermann et al., 1993; Schafer et al., 1999)]. Thus, we computed cosmogenic ${}^{21}\text{Ne}$ concentrations by assuming a two-component mixture of cosmogenic and atmospheric components. Finally, repeat analyses of the CRONUS “A” quartz standard during the period of these measurements yielded a mean of 338.6 ± 5.6 Matoms/g cosmogenic ${}^{21}\text{Ne}$.

3.4. (U-Th)/He ages of secondary goethite

In addition to measuring helium concentrations and isotopic compositions on large (~20 mg) samples, we also performed (U-Th)/He dating on few- μg size pieces of goethite from some of the hand samples from the N4 profile using standard practices (Heim et al., 2006). Dated pieces were drilled from polished sections and were chosen to represent to the maximum extent possible a single generation of pure goethite. These tiny pieces almost certainly do not have the same He age as the far larger samples analyzed for ${}^3\text{He}$. The large samples unavoidably include multiple generations of goethite and possible small residual fragments of BIF hematite. Potential complications that arise from these probable impurities are discussed below.

4. Results

4.1. Cosmogenic ${}^3\text{He}$ production rate in hematite from ${}^{21}\text{Ne}$ in coexisting quartz

Table 1 shows ${}^3\text{He}$ and ${}^4\text{He}$ concentrations in eight aliquots of hematite sample PIC-06-12 from the Pico site. The weighted mean ${}^3\text{He}$

Table 1

He measurements in hematite sample PIC-08-12.

Sample name	Aliquot	Aliquot weight (mg)	Maximum heating temperature ^a (°C)	Heating time (h)	Total ${}^4\text{He}$ released ^b (10^{12} atoms/g)	Total ${}^3\text{He}$ released ^b (10^6 atoms/g ¹)
PIC-06-12	Ab	20.5	1400	0.2	1085 \pm 54	193 \pm 17
	Ac	23.3	1400	0.2	1057 \pm 53	195 \pm 18
	Ad	3.8	1400	0.2	795 \pm 40	239 \pm 42
	Ae ^c	5.2	1500	0.2	520 \pm 26	201 \pm 29
	Af	5.2	1500	0.2	766 \pm 38	214 \pm 38
	Ag ^c	27.3	1325	0.2	702 \pm 35	220 \pm 25
	Ba	20.3	1400	0.2	678 \pm 34	197 \pm 19
	Bb	22.8	1350	0.2	883 \pm 44	201 \pm 16

Notes:

^a Followed by re-extraction at 1550 °C that was below detection limit.^b Total uncertainty includes counting uncertainties on all peaks as well as the reproducibility of He signals in the standard.^c Heated in multiple heating steps.

concentration is 201.3 ± 7.6 Matom/g (Table 1), despite a two-fold variation in the ${}^4\text{He}$ concentrations and six-fold range in mass. This is a very high concentration of ${}^3\text{He}$ compared to common minerals on the earth and so is suggestive of a cosmogenic origin in a sample with fairly long cosmic ray exposure duration. However, the ${}^3\text{He}/{}^4\text{He}$ ratios are sufficiently low that other ${}^3\text{He}$ sources are possible. The absence of correlation with ${}^4\text{He}$ (Fig. 1) argues against a trapped fluid component and the concentrations are too high (and ${}^3\text{He}/{}^4\text{He}$ ratios too low) to arise from trapped atmospheric He. The only alternative to a cosmogenic ${}^3\text{He}$ source is nuclear reactions on ${}^6\text{Li}$, but these are expected to be negligibly small in cangas (see below). Coupled with the high ${}^{21}\text{Ne}$ exposure age obtained on the quartz sample, we conclude that the ${}^3\text{He}$ in this hematite is cosmogenic.

The weighted mean cosmogenic ${}^{21}\text{Ne}$ concentration in four aliquots of quartz from PIC-06-12 is 50.9 ± 1.5 Matom/g (Table 2). Thus, given the assumptions discussed above, the observed $[{}^3\text{He}]_{\text{hematite}}/[{}^{21}\text{Ne}]_{\text{quartz}}$ ratio of 3.95 ± 0.19 is equivalent to the production ratio $P^3\text{He}_{\text{hematite}}/P^{21}\text{Ne}_{\text{quartz}}$. Currently, the cosmic-ray-produced nuclide with the best

absolute constraints on the production rate is ${}^{10}\text{Be}$; recent calibration measurements (CRONUS-Earth, unpublished data) and the production rate scaling scheme of Stone (2000) imply a reference ${}^{10}\text{Be}$ production rate at sea level and high latitude of 4.2 ± 0.2 atoms/g/yr. Balco and Shuster (2009) found that the ${}^{21}\text{Ne}/{}^{10}\text{Be}$ production ratio is 4.1 ± 0.2 . From these values, their uncertainties and our estimate of 3.95 ± 0.19 for $P^3\text{He}_{\text{hematite}}/P^{21}\text{Ne}_{\text{quartz}}$, the reference SLHL production rate for ${}^3\text{He}$ in hematite is 68.1 ± 8.1 atoms/g/yr. If any of the ${}^3\text{He}$ observed in PIC-06-12 was not cosmic-ray-produced, the ${}^3\text{He}$ production rate would be lower.

4.2. Carajás goethite (U-Th)/He ages

Goethite (U-Th)/He ages from the Carajás site support field observations of multiple episodes of Fe-oxide precipitation. The (U-Th)/He ages, which we interpret as crystallization ages, range from 0.7 to 41 Ma (Table 3). Two aliquots from each depth in the profile were analyzed, and while at several depths the two aliquots yield very similar ages, in a few cases the two differ greatly. As shown in Fig. 2, there is no systematic trend of age with depth in the profile. These observations illustrate the dynamic nature of the canga profile—ongoing dissolution and reprecipitation of goethite occurs to at least 10 m depth. As shown both by the He ages and petrographic examination, the canga is composed of many goethite generations intimately mixed even at the scale sampled for (U-Th)/He ages. The canga does not grow simply from the top downward, but instead experiences multiple stages of internal reprocessing; a similar phenomenon was observed in the Pico canga (Monteiro, 2011).

Importantly, this dissolution and reprecipitation occurred while the samples simultaneously experienced cosmic ray irradiation. Dissolution will release cosmogenic ${}^3\text{He}$ that is ultimately lost from the profile. Thus, unlike commonly analyzed cosmogenic isotope depth profiles, we cannot assume that all samples in the profile experienced the same duration of exposure. Because Fe-oxides may have precipitated at different times and may have been translocated with respect to one another within the canga, we do not necessarily expect a simple decaying exponential profile of cosmogenic ${}^3\text{He}$.

4.3. Carajás ${}^3\text{He}$ depth profile

The concentrations of ${}^3\text{He}$ and ${}^4\text{He}$ in hematite and goethite samples from the vertical depth profile from Carajás are shown in Table 4 and Fig. 3. The ${}^3\text{He}$ concentrations in both minerals roughly agree and generally decrease with increasing depth [Fig. 3(a)]. Maximum surface concentrations in goethite and hematite approach ~ 200 and ~ 300 Matom/g, respectively, and decrease to ~ 25 Matom/g at 10 m depth. The ${}^3\text{He}$ concentrations in hematite are scattered, particularly in the uppermost ~ 2 m of the profile. Although the ${}^4\text{He}$ concentrations

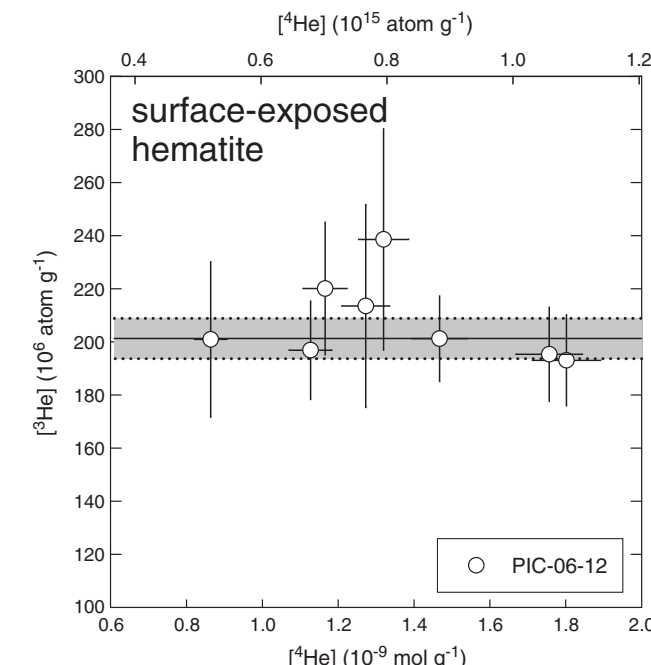


Fig. 1. Helium isotope concentrations in multiple aliquots of a surface-exposed hematite sample from the Pico iron mine in the Quadrilátero Ferrífero, Brazil. Shown are the measured ${}^3\text{He}$ and ${}^4\text{He}$ concentrations with ± 1 standard deviation. The solid horizontal line is the weighted mean of the ${}^3\text{He}$ concentration ($201.3 \pm 7.6 \times 10^6$ atom g⁻¹), with ± 1 standard deviation as dotted lines. We find no correlation between $[{}^4\text{He}]$ and $[{}^3\text{He}]$.

Table 2
Ne measurements in co-existing quartz sample PIC-06-12.

Sample name	Aliquot	Aliquot weight (g)	Heating temperature (°C)	Heating time (h)	Total ^{20}Ne released ^a (10^9 atoms)	Total ^{21}Ne released ^b (10^6 atoms)	$^{21}\text{Ne}/^{20}\text{Ne}^c$ (10^{-3})	$^{22}\text{Ne}/^{20}\text{Ne}^c$ (10^{-3})	Cosmogenic $^{21}\text{Ne}^d$ This heating step (10^6 atoms/g)	Cosmogenic ^{21}Ne ^{21}Ne as% of ^{21}Ne released in this heating step	Percent of total cosmogenic ^{21}Ne released in this step	Total ^e cosmogenic ^{21}Ne (10^6 atoms/g)
PIC-06-12A a	0.10702	390	0.2	3.215 +/- 0.068	13.402 +/- 0.456	4.165 +/- 0.096	101.9 +/- 1.1	36.37 +/- 2.99	29	71	50.9 +/- 3.6	
PIC-06-12A b	0.07391	1140	0.2	1.322 +/- 0.031	5.468 +/- 0.242	4.133 +/- 0.154	104.7 +/- 1.8	14.56 +/- 1.94	28	29	0	
PIC-06-12A c	0.1346	390	0.2	0.055 +/- 0.012	0.215 +/- 0.052	3.884 +/- 1.272	126.4 +/- 35.4	-+/- -	39	78	53.5 +/- 3.9	
PIC-06-12A d	0.1235	780	0.2	1.633 +/- 0.037	7.910 +/- 0.303	4.841 +/- 0.145	103.6 +/- 1.8	41.71 +/- 3.35	24	22		
		1140	0.2	0.942 +/- 0.025	3.661 +/- 0.164	3.883 +/- 0.154	101.8 +/- 2.3	11.82 +/- 1.99				
		390	0.2	0.034 +/- 0.010	0.140 +/- 0.038	4.058 +/- 1.649	123.3 +/- 48.7	-+/- -				
		780	0.2	2.286 +/- 0.039	12.455 +/- 0.376	5.431 +/- 0.132	102.7 +/- 1.6	42.14 +/- 2.36	46	82	51.5 +/- 2.8	
		1140	0.2	1.670 +/- 0.022	6.202 +/- 0.237	3.708 +/- 0.122	102.1 +/- 1.6	9.32 +/- 1.52	20	18		
		390	0.2	0.074 +/- 0.014	0.170 +/- 0.049	2.318 +/- 0.795	117.8 +/- 26.1	-+/- -	0	0	49.5 +/- 2.4	
		780	0.2	2.092 +/- 0.023	10.451 +/- 0.254	4.963 +/- 0.097	104.2 +/- 1.4	34.07 +/- 1.69	40	69		
		1140	0.2	1.695 +/- 0.018	6.930 +/- 0.235	4.077 +/- 0.124	105.1 +/- 1.7	15.39 +/- 1.72	27	31		
		390	0.2	0.080 +/- 0.011	0.239 +/- 0.048	2.955 +/- 0.070	93.6 +/- 23.2	-+/- -	0			

^a Computed by comparison to ^{20}Ne signal in air pipettes. 1-sigma uncertainty includes measurement uncertainty of ^{20}Ne signal in this analysis and the reproducibility of the air pipette signal.

^b Computed by comparison to ^{21}Ne signal in air pipettes. 1-sigma uncertainty includes measurement uncertainty of ^{21}Ne signal in this analysis and the reproducibility of the air pipette signal.

^c Isotope ratio measured internally during each analysis; does not involve normalization to the Ne isotope signals in the air pipettes.

^d Analyses where cosmogenic ^{21}Ne was not distinguishable from zero at 1 sigma are not shown. Cosmogenic ^{21}Ne concentrations were calculated by normalization to either the ^{20}Ne or ^{21}Ne signal in the air pipettes, depending on which method yielded better precision.

^e Total uncertainty includes counting uncertainties on all peaks as well as the reproducibility of Ne signals in the air standard.

show no clear relationship with depth, the ^4He concentrations in hematite are systematically higher than in goethite [Fig. 3(b)].

5. Discussion

5.1. Production rate of cosmogenic ^3He in hematite and goethite

Our empirical ^3He production rate is in good agreement with predictions for Fe_2O_3 from the model of (Masarik, 2002) (66 atom/g/yr) and the observations of chemically similar phases by (Bryce and Farley, 2002) and (Margerison et al., 2005) (~70 atom/g/yr), but clearly differs from that of (Kober et al., 2005) (123 atom/g/yr). It is important to note that the possible presence of non-cosmogenic ^3He in our hematite would result in an overestimation (rather than underestimation) of the ^3He production rate. At present we have no explanation for this discrepancy, but we note that Kober et al.'s results also predict ^3He production rates in olivine and pyroxene far higher than others have observed [e.g., (Fenton et al., 2009)].

Although the model predictions of Masarik (2002) and Kober et al. (2005) differ in absolute production rates, they agree well in the production ratio predicted for $\text{FeOOH}/\text{Fe}_2\text{O}_3$. The predicted ratios $P^3\text{He}_{\text{goethite}}/P^3\text{He}_{\text{hematite}}$ of 1.07 (Masarik, 2002) and 1.04 (Kober et al., 2005), indicate that the ^3He production rate in goethite should be ~5% higher than in hematite or ~72 atom/g/yr at SLHL.

5.2. Carajás goethite He ages

We note two curious features of the (U-Th)/He data from the N4C profile. First, the U and Th concentrations tend to increase with depth (Table 3). This suggests that the solution-reprecipitation process may "leak" U and Th from the profile in percolating groundwater, and the samples near the surface have experienced more such cycles and hence are less radioactive. Second, there is a notable positive correlation between (U-Th)/He age and U/Th ratio. One possible explanation for this observation is that the leakage preferentially removes U, leaving a lower U/Th ratio in the profile through time (Dequincey et al., 2002). Further study is required to evaluate this speculative explanation. We do not expect that the goethite (U-Th)/He ages of very small aliquots (Table 3) accurately record the age of the larger (probably polygenerational) aliquots analyzed for ^3He (Table 4).

5.3. Carajás ^3He depth profile

In the following, we discuss three aspects of the observed depth profile. First, high ^3He concentrations at the surface are presumably cosmogenic in origin. Thus, having estimated the surface ^3He production rate, we can use these concentrations to estimate the surface erosion rate. Second, samples between 1 and 10 m depth have significantly more ^3He than expected from spallation alone. We discuss the possibilities that this could be due to translocation of samples in the canga or production by cosmic ray muons. Third, hematites from >80 m depth contain a measurable abundance of ^3He that is not due to cosmic ray interactions (Table 4). We therefore also discuss possible sources of non-cosmogenic ^3He .

If cosmogenic nuclide production is predominantly by high-energy spallation and a surface is experiencing steady erosion, the erosion rate is related to the surface nuclide concentration by $\dot{\epsilon} = P\Lambda/N$, where $\dot{\epsilon}$ is the erosion rate ($\text{g}/\text{cm}^2/\text{yr}$), P is the production rate ($\text{atoms}/\text{g}/\text{yr}$), Λ is an attenuation lengthscale of cosmogenic production [$160 \text{ g}/\text{cm}^2$; see (Gosse and Phillips, 2001) for discussion], and N is the nuclide concentration (atom/g) observed at the surface (Dunai, 2010; Lal, 1991). When scaled to the Carajás depth profile site (~6° S, 720 m elevation) according to (Stone, 2000), our estimated ^3He production rates for hematite and goethite are ~70 and ~74 atom/g/yr, respectively. These values, with appropriate corrections for sample depth, an assumed density of $2.7 \text{ g}/\text{cm}^3$, and the ^3He concentrations observed in

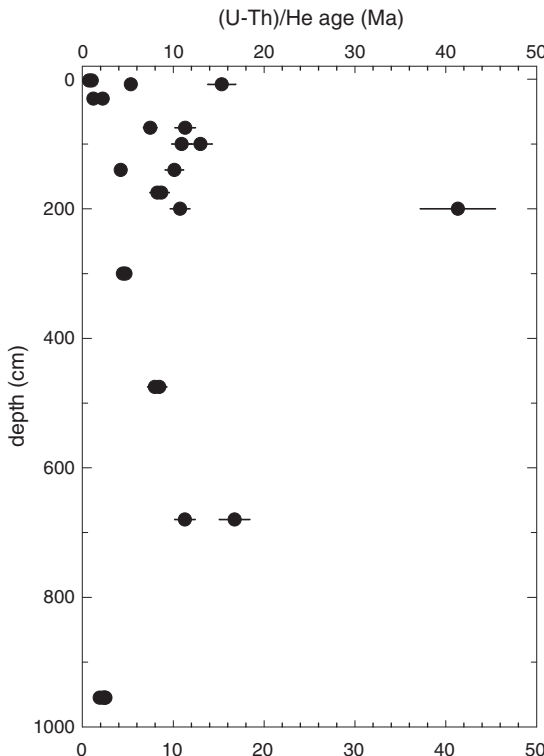
Table 3

(U-Th)/He measurements in goethite samples from N4C depth profile.

	Depth (cm)	Aliquot	Aliquot mass (10^{-6} g)	U (ppm)	Th (ppm)	Total ${}^4\text{He}$ released (10^{-9} mol g $^{-1}$)	(U-Th)/He age ^a (Ma)
Goethite	2	a	71	0.13	1.99	0.0024	0.73
	2	b	109	0.10	1.70	0.0028	1.02
	8	a	97	0.48	1.92	0.0779	15.33
	8	b	93	0.41	2.52	0.0290	5.33
	30	a	116	0.39	2.67	0.0124	2.23
	30	b	50	0.25	1.88	0.0046	1.21
	75	a	80	1.50	4.42	0.1562	11.31
	75	b	87	1.36	3.12	0.0851	7.46
	100	a	26	2.25	9.51	0.2667	10.92
	100	b	65	1.95	8.41	0.2774	12.99
	140	a	89	0.82	4.74	0.0444	4.22
	140	b	88	0.87	5.98	0.1252	10.12
	175	a	95	0.51	2.94	0.0539	8.25
	175	b	80	0.82	2.88	0.0707	8.68
	200	a	13	1.37	5.09	0.5775	41.33
	200	b	88	2.12	10.25	0.2652	10.75
	300	a	52	1.11	7.60	0.0747	4.74
	300	b	96	1.43	10.50	0.0945	4.46
	475	a	79	5.90	23.04	0.4912	7.98
	475	b	77	5.68	23.66	0.5167	8.45
	680	a	90	1.16	2.98	0.1142	11.27
	680	b	83	1.79	6.96	0.3122	16.74
	955	a	37	3.25	27.92	0.1353	2.54
	955	b	66	3.13	29.89	0.1269	2.30
	955	c	91	2.58	15.11	0.0633	1.90
	955	d	68	2.98	14.82	0.0866	2.46

^a Age uncertainty is estimated to be $\pm 10\%$.

the near-surface hematite samples (ranging from 83 to 256 Matom/g after subtracting for a background of 11 Matom/g, as discussed below) imply steady-state erosion rates of 0.13–0.46 m/Myr. The ${}^3\text{He}$ in the surface goethite sample (177 Matom/g, corrected for background) implies a steady-state erosion rate of 0.2 m/Myr. These calculations assume that ${}^3\text{He}$ produced by deeply penetrating muons is negligible.

**Fig. 2.** Goethite (U-Th)/He ages collected along the N4C vertical depth profile from Carajás, Brazil plotted against depth below the modern surface.

Below, we discuss the possibility that significant ${}^3\text{He}$ production by muons may explain observed ${}^3\text{He}$ concentrations at depth; if this were the case, these calculations would underestimate the true erosion rates (Balco et al., 2008; Granger et al., 2001; Stone et al., 1998).

Although the ${}^3\text{He}$ concentrations in both minerals generally decrease with increasing depth, we find ${}^3\text{He}$ concentrations at depths > 1 m that are significantly higher than predicted solely for spallogenic production (Fig. 4). An attenuation lengthscale for ${}^3\text{He}$ production by spallation reactions of 160 g/cm 2 (Dunai, 2010) predicts that by a depth of ~ 2 m, the ${}^3\text{He}$ concentration should be less than 1/10 of the surface concentration, or ~ 20 Matom/g. However, the ${}^3\text{He}$ concentrations do not approach this concentration until a depth of ~ 10 m. One possible explanation is that these samples contain significant muon-produced ${}^3\text{He}$. Alternatively, the fact that the ${}^3\text{He}$ concentrations do not monotonically decrease with depth – particularly in the uppermost ~ 2 m – suggests that the duricrust may be a chemically or physically dynamic environment over million-year timescales. If so, high ${}^3\text{He}$ concentrations at depth could have resulted from vertical mixing.

The two hematite samples from 81 to 131 m (Table 4) depth were shielded from cosmic rays since deposition. Therefore, the observed ${}^3\text{He}$ concentrations at these depths (~ 6 and ~ 16 Matom/g, respectively) provide an estimate of the non-cosmogenic background ${}^3\text{He}$ concentration at this site, and indicate that the background abundances may vary between samples. Although this ${}^3\text{He}$ is clearly non-cosmogenic, its origin is unclear. Also, it is not clear that the background ${}^3\text{He}$ present in these samples is also present in canga samples < 10 m below the surface. Nevertheless as an upper limit we assume that all samples contain 11 Matom/g of non-cosmogenic ${}^3\text{He}$, or $\sim 4\%$ of the maximum surface concentration.

5.4. Potential sources of ${}^3\text{He}$ at 2–10 m depth

The ${}^3\text{He}$ that cannot be explained by spallation reactions at 2–10 m depth may be explained by production by cosmic ray muons, or by translocation of surface material with prior exposure to greater depth. In this section we consider both possibilities.

Table 4

He measurements in hematite and goethite samples from N4C depth profile.

	Depth (cm)	Aliquot	Aliquot mass (mg)	Maximum heating temperature ^a (°C)	Heating time (h)	Total ${}^4\text{He}$ released ^b (10^{12} atoms/g)	Total ${}^3\text{He}$ released ^b (10^6 atoms/g)
Hematite	5	a ^c	15.7	1400	0.5	171.7 +/− 0.3	94 +/− 25
	5	b	6.9	1400	0.5	61.9 +/− 0.5	184 +/− 27
	12	a ^c	21.1	1400	0.5	229.2 +/− 0.3	255 +/− 42
	12	b	10.3	1400	0.5	105.3 +/− 0.2	267 +/− 26
	30	a ^c	15.0	1400	0.5	2133.0 +/− 1.5	135 +/− 34
	40	a ^c	24.3	1400	0.5	145.9 +/− 0.1	300 +/− 30
	75	a	21.7	1400	0.5	115.2 +/− 0.1	224 +/− 19
	100	a	21.7	1400	0.5	156.9 +/− 0.2	152 +/− 16
	140	a	22.7	1400	0.5	8.4 +/− 0.3	29 +/− 10
	175	a	8.2	1400	0.5	156.5 +/− 0.5	82 +/− 18
	200	a ^c	18.0	1400	0.5	203.5 +/− 0.2	145 +/− 18
	300	a	24.0	1400	0.5	152.9 +/− 0.1	87 +/− 11
	475	a	20.0	1400	0.5	50.7 +/− 0.3	49 +/− 8
	680	b	23.9	1400	0.5	178.9 +/− 0.2	83 +/− 33
	955	a	23.2	1400	0.5	40.1 +/− 0.1	53 +/− 11
	955	b	18.1	1400	0.5	22.3 +/− 0.1	26 +/− 7
	8105	a	48.8	1400	0.5	n.d.	6 +/− 2
	13,070	a	49.9	1400	0.5	n.d.	16 +/− 4
Goethite	12	a	7.9	1000	0.3	49.5 +/− 0.5	188 +/− 27
	75	a	3.9	1000	0.3	32.5 +/− 1.2	168 +/− 41
	140	a	26.1	1000	0.3	37.1 +/− 0.2	125 +/− 11
	175	a	16.0	1000	0.3	48.6 +/− 0.2	120 +/− 15
	300	a	19.7	1000	0.3	30.7 +/− 0.3	67 +/− 9
	680	a	17.6	1000	0.3	52.1 +/− 0.1	38 +/− 8
	955	a	13.2	1000	0.3	28.6 +/− 0.1	26 +/− 8

Notes:

n.d. is not determined.

^a Followed by re-extraction at 1500 °C (hematite) or 1000 °C (goethite) that was below detection limit.^b Total uncertainty includes counting uncertainties on all peaks as well as the reproducibility of He signals in the standard.^c Heated in multiple heating steps.

First we consider whether the form of the observed depth profile is compatible with muon production. The ${}^3\text{He}$ concentration in a deep sample can be estimated from the muon flux at depth, the effective cross section for a set of ${}^3\text{He}$ -producing muon reactions, and the

total duration of exposure. Although neither the cross sections nor the exposure duration is independently known, we can choose plausible values of these parameters to predict the form of a depth profile with a significant amount of ${}^3\text{He}$ produced by muon reactions.

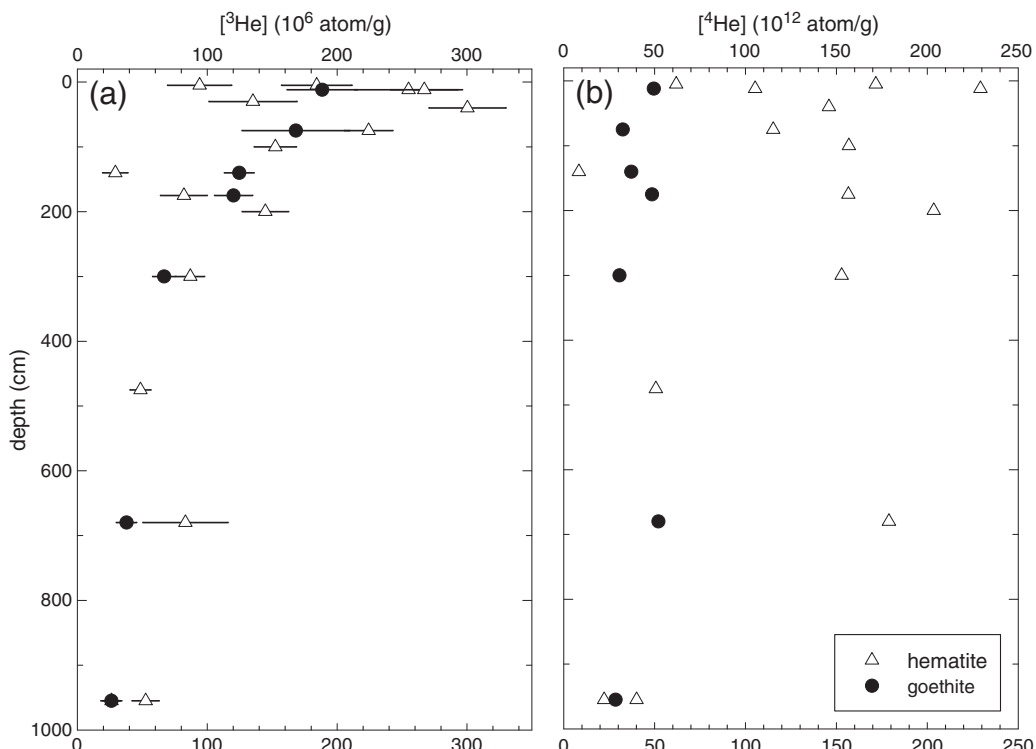


Fig. 3. Helium isotope concentrations in goethite and hematite samples collected along a vertical depth profile (in the N4C deposit) from Carajás, Brazil. Shown are the measured ${}^3\text{He}$ (a) and ${}^4\text{He}$ (b) concentrations in both phases plotted against depth below the modern surface.

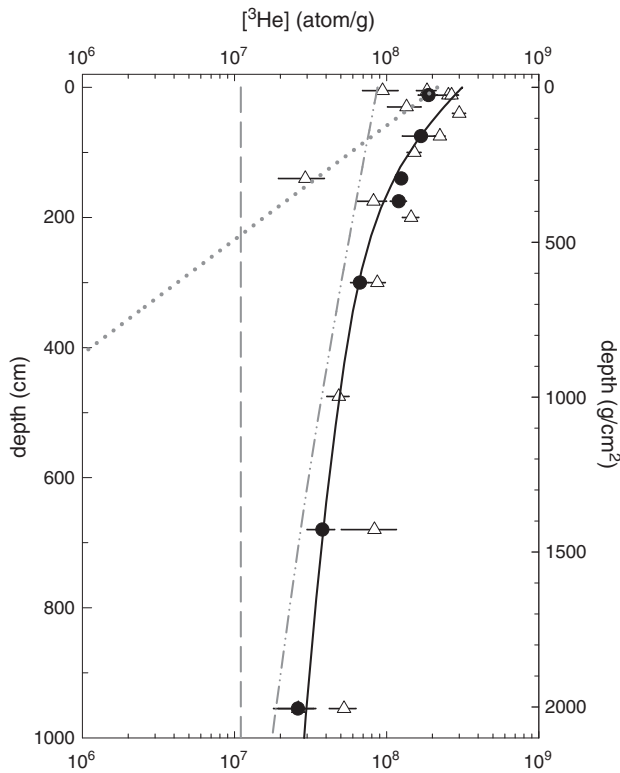


Fig. 4. A model of cosmogenic ${}^3\text{He}$ production as a function of depth and surface erosion. Observed ${}^3\text{He}$ concentrations in goethite (circles) and hematite (diamonds) are as shown in Fig. 3. The solid curve was calculated assuming a total ${}^3\text{He}$ production rate of 74.2 atoms/g/yr in goethite [i.e., our SLHL rate scaled to 6° S and 700 m elevation, using Stone (2000)], of which 5 atoms/g/yr is due to muon and an erosion rate of ~25 cm/Myr (i.e., 52 g/cm²/Myr; as suggested by the ${}^3\text{He}$ concentration in near surface goethite) for a duration of 20 Myr since many goethite (U-Th)/He ages approach 20 Ma. The curve was calculated by summing ${}^3\text{He}$ from three sources: (i) the ${}^3\text{He}$ concentration due to spallation reactions with an attenuation lengthscale of 160 g/cm² (dotted line), (ii) the ${}^3\text{He}$ due to muon reactions (dash-dot line), and (iii) a background (i.e., non-cosmogenic) ${}^3\text{He}$ concentration of 11 Matom/g (dashed line). We computed subsurface muon fluxes according to the method of Heisinger et al. (2002a,b); as implemented in Balco et al. (2008), and prescribed arbitrary muon interaction cross sections to obtain a predicted depth-concentration profile resembling the observations. These are: 300 pbarn and 100 pbarn cross-sections for ${}^3\text{He}$ production by fast muon interactions at 190 GeV on Fe and O respectively; and total likelihoods for ${}^3\text{He}$ emission following negative muon capture of 0.025 and 0.0012 for Fe and O, respectively. The total likelihood is the product $f_c \times f_D \times f^*$ of Heisinger et al. (2002a) and Heisinger et al. (2002b); f_c is the fraction of muons interacting with the target nucleus, f_D is the probability that the negative muon does not decay before nuclear capture, and f^* is the effective probability of ${}^3\text{He}$ production after negative muon capture. These cross-sections imply that ~7% of total surface ${}^3\text{He}$ production at this site is due to muons.

Fig. 4 shows a predicted ${}^3\text{He}$ concentration-depth profile assuming steady surface erosion and subsurface production by spallation and muon interactions. Because we do not know the total exposure age of these samples, the assumed muon interaction cross-section values are guesses rather than estimates, and are significantly higher than have been measured for other commonly measured cosmogenic nuclides. We are unaware of any experimental constraints on these values, but because ${}^3\text{He}$ is light compared to these nuclides, it appears plausible that muon interaction cross-sections could be higher.

The form of the depth profile predicted by these assumptions is consistent with the measured depth profile (Fig. 4). Thus, we find no evidence against the hypothesis that significant concentrations of subsurface ${}^3\text{He}$ were produced by muon interactions. If the subsurface ${}^3\text{He}$ is due to muon production, the observations require a long duration of low erosion rate, unless our assumed muon interaction cross sections are grossly underestimated. As these cross-sections are already high relative to those for other cosmogenic nuclides, this is unlikely.

Although muon production provides one possible explanation of high ${}^3\text{He}$ concentrations at depth, it is possible that these high concentrations instead represent samples of material that once resided closer to the surface (i.e., in the zone of spallogenic production) and have been transported downward into the weathering profile, perhaps by bioturbation such as root wedging. Downward translocation of silt- and clay-sized material is well documented in soil and regolith, and is responsible for, among other things, the presence of ${}^{10}\text{Be}$ derived from atmospheric fallout at several meters depth in saprolite ([Graly et al., 2010] and references therein]. However, we have measured ${}^3\text{He}$ in individual Fe-oxide particles, not the bulk average ${}^3\text{He}$ concentration at certain depths.

5.5. Potential sources of non-cosmogenic ${}^3\text{He}$ in shielded samples

The ${}^3\text{He}$ observed in samples from 81 to 131 m depth appears to constitute a background ${}^3\text{He}$ component that cannot have been produced by cosmic ray interactions or be the result of particle translocation. Helium-3 can be produced in minerals by several nuclear reactions and may also be incorporated into Fe-oxides from different sources. In this section, we consider the magnitude of several possible sources of ${}^3\text{He}$ that could explain these results.

5.5.1. Cosmic dust

A high flux of ${}^3\text{He}$ is delivered to oceanic sediments in the form of interplanetary dust particles (IDPs) (Farley, 1995; Merrihue, 1964; Ozima et al., 1984). Thus extraterrestrial ${}^3\text{He}$ could have been incorporated into primary iron oxides when the BIF was deposited at ~2745 Ma (Klein and Ladeira, 2002; Trendall et al., 1998). However, for such ${}^3\text{He}$ to be observed today, it would need to have been retained over the life of the deposit. The Carajas formation has experienced greenschist facies metamorphism (to ~400–500 °C), most likely at ~1880 Ma (Machado et al., 1991; Teixeira and Eggler, 1994). The kinetics of ${}^3\text{He}$ diffusion in phases that host extraterrestrial ${}^3\text{He}$ predicts complete diffusive loss at these temperatures (Mukhopadhyay and Farley, 2006).

5.5.2. Nucleogenic ${}^3\text{He}$ produced from Li

The chemical composition of canga is not conducive to the production of nucleogenic ${}^3\text{He}$ from the reaction ${}^6\text{Li}(\text{n},\alpha){}^3\text{H} \rightarrow {}^3\text{He}$. The rate at which ${}^3\text{He}$ is produced by this reaction depends on the Li concentration of the sample and on the production rate of neutrons and the abundance of elements that compete with Li for the absorption of neutrons in the rock. In the case of canga, Li contents are low, the neutron production rate is low, and the abundance of competing neutron absorbers is fairly high.

As discussed by Andrews and Kay (1982), the production rate of neutrons in a rock depends mainly on the concentration of U and Th and of light elements with high (α,n) cross sections such as Na, Al, Mg, and Si. Canga has very low concentrations of these elements. We modified the equation of Andrews and Kay (1982) to include the ordinarily negligible production of neutrons from α -capture by Fe and O using the production rates from Feige et al. (1968). For the bulk chemical composition of canga we used data from Pico from Ramanaidou (2009). We adopted the mean U and Th concentrations of the N4C goethite samples of 1.7 and 8.9 ppm, respectively. These values yield a neutron production rate of ~1.5 n/g/yr, which is about an order of magnitude lower than in typical granite.

To compute the fraction of these neutrons absorbed on Li, we again assumed the bulk canga composition from Ramanaidou (2009). Several trace elements have unusually high neutron capture cross sections (e.g., B, Gd) yet we do not have measurements for these elements. Rather than guess values for them we assume the concentration of all absorbers other than Li and the well-determined major elements Fe, Al, Si, and O are negligible. This will yield an upper limit to the production rate of ${}^3\text{He}$ from ${}^6\text{Li}$.

Table 5 shows Li concentrations in our samples. Goethites from the N4 depth profile above 10 m depth and the surface sample at Pico have low Li contents, averaging ~90 ppb. This concentration coupled with the neutron production and absorption characteristics described above yields a ${}^3\text{He}$ production rate of 46 atom/g/Myr. This is an extraordinarily low production rate. Even if all of the ${}^3\text{He}$ produced since the BIF was deposited at ~2745 Ma (Klein and Ladeira, 2002; Trendall et al., 1998) were retained, just 0.1 Matom/g of nucleogenic ${}^3\text{He}$ would be present in the canga. Thus, ${}^3\text{He}$ production on Li clearly cannot explain observed concentrations at <10 m depth in the Carajás depth profile that we have attributed above to either muon production or particle translocation.

The shielded samples from 81 to 131 m at Carajas, presumably because they are less chemically leached, have higher Li concentrations (170 and 890 ppm respectively). If these samples also have proportionally higher concentrations of neutron-producing light elements (Klein and Ladeira, 2002), ${}^3\text{He}$ production from ${}^6\text{Li}$ could be more than an order of magnitude higher, potentially accounting for a significant fraction of the ~11 Matom/g of ${}^3\text{He}$ they carry. Evaluating this possibility requires several quantities we do not yet know, including the He retention age of the BIF hematite, the concentration of U and Th, concentrations of neutron producers and absorbers, and the relative distribution of elements involved in (α, n) reactions.

5.6. Stability of chemical weathering profiles

Our estimate of the cosmogenic ${}^3\text{He}$ production rate in goethite and hematite allows us to assess the long-term stability of the canga by quantifying the surface erosion rate. Two basic conclusions about the Carajás canga arise from the observed ${}^3\text{He}$ concentrations and the goethite (U-Th)/He ages throughout the profile: (i) the Fe-oxide duricrust has experienced less than 1 m of surface erosion per million years, and (ii) the duricrust has been exposed to cosmic ray-induced ${}^3\text{He}$ production for a very long duration, possibly more than 20 My, as indicated by the oldest goethite (U-Th)/He ages. These interpretations support the geomorphic observation that high-standing plateaus of the region are associated with Fe-rich duricrusts, which qualitatively indicates that the canga has been relatively resistant to physical erosion (Dorr, 1964; Klein and Ladeira, 2002). A low erosion rate of Fe-rich canga suggests that, once formed, the hard duricrust provides an armoring effect that preserves the deeply-weathered, more unconsolidated rocks beneath it. Therefore, this effect has defined the local topography over the long term.

Previous studies have found significantly higher rates of erosion (2–9 m/Myr) from ${}^{10}\text{Be}$ observations in lateritic profiles in tectonically stable settings in other regions (Braucher et al., 1998a, 1998b; Brown et al., 1994). Although factors such as local climate and lithology influence both the development and preservation of lateritic profiles, we note that these previous studies investigated lateritic profiles that are not capped by Fe-rich duricrusts. The much lower

erosion rate at Carajás suggests that it is the high concentration of Fe in the system that has led to its preservation.

The very low rates of erosion (~0.13–0.46 m/Myr) at Carajás are especially noteworthy given the site's presently high rainfall rate (~1500 mm/yr). This provides a clear example of a very low rate of erosion at a site with essentially zero tectonic activity, but high rainfall. Interestingly, Brown et al. (1994) concluded that much higher erosion rates of 3–8 m/Myr observed in West Africa resulted from a transition to the present-day dry climate of that region that "stabilized" and preserved the lateritic system. This simple comparison between sites suggests that local rainfall is not the primary control on preservation of lateritic profiles.

However, despite the remarkable stability of the Carajás canga, we also find evidence that the system has been physically and/or chemically dynamic over million-year timescales. The ${}^3\text{He}$ concentrations do not all follow a systematic decrease with depth, particularly near the present surface (Fig. 3). For example, some hematite aliquots (e.g., from 5 and 30 cm depths) have ${}^3\text{He}$ concentrations that are significantly less than proximal samples, while the sample from 140 cm has a concentration that is significantly lower than in all other goethite and hematite samples collected between 100 and 200 cm. Conversely, the hematite sample at 680 cm has a ${}^3\text{He}$ concentration that is more consistent with hematite and goethite samples at 200–300 cm. These observations suggest that positions of at least some oxides have changed relative to one another and to the surface over time, for example due to biological activity such as deeply penetrating tree roots, expansion fracturing of the canga, or translocation associated with burying insects such as ants and termites. Conversely, the low ${}^3\text{He}$ concentrations of some minerals in the uppermost 2 m of the profile (Fig. 4) may reflect more recent precipitation than nearby samples.

Such complexity and episodic precipitation events are expected if the redox state within the profile had changed over time due to long-term variability in climate or permeability (Cornu et al., 2009). For example, transport of organic matter into the profile could provide locally wet and reducing conditions under which Fe-oxides dissolve. If the resulting solution migrates into an oxic zone, a secondary Fe-oxide would precipitate. Even if the canga has remained intact for millions of years, it may be expected that multiple generations of dissolution and re-precipitation have occurred. In principle, this preserved complexity provides a record of the local aridity, humidity, biological activity and chemistry over millions of years.

6. Conclusions

Our estimate of the cosmogenic ${}^3\text{He}$ production rates in goethite and hematite provides a tool with which to constrain the surface exposure age of these minerals, and to study the stability and dynamics of deep chemical weathering profiles that complements techniques that establish crystallization ages. Our initial application of this approach to study a Fe-rich canga atop the deeply weathered Carajás banded iron formation reveals a very low erosion rate in a tropical setting that is both tectonically stable and has experienced abundant rainfall. Because non-cosmogenic ${}^3\text{He}$ is not likely to occur in the Fe-oxides of the Carajás canga, the oxides are well-suited for cosmogenic ${}^3\text{He}$ measurements. A depth profile of ${}^3\text{He}$ concentrations suggests either that a significant proportion of cosmogenic ${}^3\text{He}$ may be produced by nuclear reactions induced by muons, or that there is significant downward transport of Fe-oxide particles that were previously exposed near the surface.

Acknowledgments

We thank Vale S.A. for providing us access to the sampling sites at Carajás, Carlos Spier (then at MBR) for providing access and field support for sampling that the Pico Mine, and M. Honda and P.-H. Blard for constructive reviews of the manuscript. Funding was provided by the following sources: UQ-AGES for funding the field sampling exercises

Table 5
Li concentrations in goethite and hematite samples.

	Depth (cm)	Aliquot mass (mg)	Li (ppb)
Goethite (Pico)	0	2.8	37
	500	1.6	85
	1000	1.5	99
Goethite (Carajas)	12	1.4	54
	30	1.7	156
	75	3.3	36
	100	1.6	105
	475	1.1	71
	680	1.7	71
Hematite (Carajas)	965	1.3	84
	8105	1.4	168
	13,070	2.0	887

at Carajás and Pico, grants NSF-EAR-0738474 (to DLS) and NSF-EAR-0921295 (to KAF), and the Ann and Gordon Getty Foundation.

References

- Anderson, S.P., Dietrich, W.E., Brimhall, G.H., 2002. Weathering profiles, mass-balance analysis, and rates of solute loss: linkages between weathering and erosion in a small, steep catchment. *Geol. Soc. Am. Bull.* 114, 1143–1158.
- Andrews, J.N., Kay, R.L.F., 1982. Natural production of tritium in permeable rocks. *Nature* 298, 361–363.
- Balco, G., Shuster, D.L., 2009. Production rate of cosmogenic ^{21}Ne in quartz estimated from ^{10}Be , ^{26}Al , and ^{21}Ne concentrations in slowly eroding Antarctic bedrock surfaces. *Earth Planet. Sci. Lett.* 281, 48–58.
- Balco, G., Stone, J.O., Lifton, N.A., Dunai, T.J., 2008. A complete and easily accessible means of calculating surface exposure ages or erosion rates from ^{10}Be and ^{26}Al measurements. *Quat. Geochronol.* 3, 174–195.
- Beisiegel, V.R., 1982. Distrito ferrífero da Serra dos Carajás. Simpósio de Geologia da Amazônia. Sociedade Brasileira de Geologia, Belém, pp. 21–46.
- Braucher, R., Bourles, D.L., Colin, F., Brown, E.T., Boulange, B., 1998a. Brazilian laterite dynamics using in situ-produced ^{10}Be . *Earth Planet. Sci. Lett.* 163, 197–205.
- Braucher, R., Colin, F., Brown, E.T., Bourles, D.L., Bamba, O., Raisbeck, G.M., Yiou, F., Koud, J.M., 1998b. African laterite dynamics using in situ-produced Be-10. *Geochim. Cosmochim. Acta* 62, 1501–1507.
- Braucher, R., Bourles, D.L., Brown, E.T., Colin, F., Muller, J.-P., Braun, J.J., Delaune, M., Edou Minko, A., Lescouet, C., Raisbeck, G.M., Yiou, F., 2000. Application of in situ-produced cosmogenic ^{10}Be and ^{26}Al to the study of lateritic soil development in tropical forest; theory and examples from Cameroon and Gabon. *Chem. Geol.* 170, 95–111.
- Brimhall, G.H., Christopher, J.L., Ford, C., Bratt, J., Taylor, G., Warin, O., 1991. Quantitative geochemical approach to pedogenesis: importance of parent material reduction, volumetric expansion, and eolian influx in lateritization. *Geoderma* 51, 51–91.
- Brown, E.T., Bourles, D.L., Colin, F., Sanfo, Z., Raisbeck, G.M., Yiou, F., 1994. The development of iron crust lateritic systems in Burkina Faso, West Africa examined with in-situ-produced cosmogenic nuclides. *Earth Planet. Sci. Lett.* 124, 19–33.
- Bryce, J.G., Farley, K.A., 2002. ^3He exposure dating of magnetite. *Geochim. Cosmochim. Acta* 66, A108.
- Carson, M.A., Kirkby, M.J., 1972. Hillslope Form and Process. Cambridge University Press, Cambridge, UK.
- Cornu, S., Montagne, D., Vasconcelos, P.M., 2009. Dating constituent formation in soils to determine rates of soil processes: a review. *Geoderma* 153, 293–303.
- Dequincey, O., Chabaux, F., Clauer, N., Sigmarsson, O., Lievig, N., Leprun, J.C., 2002. Chemical mobilizations in laterites: evidence from trace elements and ^{238}U – ^{234}U – ^{230}Th disequilibrium. *Geochim. Cosmochim. Acta* 66, 1197–1210.
- Dorr, J.V.N., 1964. Supergene iron ores of Minas Gerais, Brazil. *Econ. Geol.* 59, 1203.
- Dunai, T.J., 2010. Cosmogenic Nuclides: Principles, Concepts and Applications in the Earth Surface Sciences. Cambridge University Press.
- Farley, K.A., 1995. Cenozoic variations in the flux of interplanetary dust recorded by ^3He in a deep sea sediment. *Nature* 376, 153–156.
- Feige, Y., Oltman, B.G., Kastner, J., 1968. Production rates of neutrons in soils due to natural radioactivity. *J. Geophys. Res.* 73, 3135–3142.
- Fenton, C.R., Niedermann, S., Goethals, M.M., Schneider, B., Wijbrans, J., 2009. Evaluation of cosmogenic ^3He and ^{21}Ne production rates in olivine and pyroxene from two Pleistocene basalt flows, western Grand Canyon, AZ, USA. *Quat. Geochronol.* 4, 475–492.
- Gosse, J.C., Phillips, F.M., 2001. Terrestrial in situ cosmogenic nuclides: theory and application. *Quat. Sci. Rev.* 20, 1475–1560.
- Graly, J.A., Bierman, P.R., Reusser, L.J., Pavich, M.J., 2010. Meteoric ^{10}Be in soil profiles—a global meta-analysis. *Geochim. Cosmochim. Acta* 74, 6814–6829.
- Granger, D.E., Riebe, C.S., Kirchner, J.W., Finkel, R.C., 2001. Modulation of erosion on steep granitic slopes by boulder armoring, as revealed by cosmogenic ^{26}Al and ^{10}Be . *Earth Planet. Sci. Lett.* 186, 269–281.
- Harder, E.C., Chamberlin, R.T., 1915. The geology of central Minas Geraes, Brazil. *J. Geol.* 23, 385–424.
- Heim, J.A., Vasconcelos, P.M., Shuster, D.L., Farley, K.A., Broadbent, G., 2006. Dating palaeochannel iron ore by (U-Th)/He analysis of supergene goethite, Hamersley Province, Australia. *Geology* 34, 173–176.
- Heisinger, B., Lal, D., Jull, A.J.T., Kubik, P., Ivy-Ochs, S., Knie, K., Nolte, E., 2002a. Production of selected cosmogenic radionuclides by muons: 2. Capture of negative muons. *Earth Planet. Sci. Lett.* 200, 357–369.
- Heisinger, B., Lal, D., Jull, A.J.T., Kubik, P., Ivy-Ochs, S., Neumaier, S., Knie, K., Lazarev, V., Nolte, E., 2002b. Production of selected cosmogenic radionuclides by muons: 1. Fast muons. *Earth Planet. Sci. Lett.* 200, 345–355.
- James, H.L., 1983. Distribution of banded iron-formation in space and time. *Dev. Precambrian Geol.* 6, 471–490.
- Klein, C., Ladeira, E.A., 2002. Petrography and geochemistry of the least altered banded iron-formation of the Archean Carajás formation, northern Brazil. *Econ. Geol. Bull. Soc. Econ. Geol.* 97, 643–651.
- Kober, F., Ivy-Ochs, S., Leya, I., Baur, H., Magna, T., Wieler, R., Kubik, P.W., 2005. In situ cosmogenic ^{10}Be and ^{21}Ne in sandstone and in situ cosmogenic ^3He in Fe-Ti-oxide minerals. *Earth Planet. Sci. Lett.* 236, 404–418.
- Kohl, C.P., Nishizumi, K., 1992. Chemical isolation of quartz for measurement of in-situ-produced cosmogenic nuclides. *Geochim. Cosmochim. Acta* 56, 3583–3587.
- Lal, D., 1991. Cosmic ray labeling of erosion surfaces: in situ nuclide production rates and erosion models. *Earth Planet. Sci. Lett.* 104, 424–439.
- Li, J.W., Vasconcelos, P., 2002. Cenozoic continental weathering and its implications for the palaeoclimate: evidence from ^{40}Ar / ^{39}Ar geochronology of supergene K-Mn oxides in Mt Tabor, central Queensland, Australia. *Earth Planet. Sci. Lett.* 200, 223–239.
- Li, J.W., Vasconcelos, P., Duzgoren-Aydin, N., Yan, D.R., Zhang, W., Deng, X.D., Zhao, X.F., Zeng, Z.P., Hu, M.A., 2007. Neogene weathering and supergene manganese enrichment in subtropical South China: an ^{40}Ar / ^{39}Ar approach and paleoclimatic significance. *Earth Planet. Sci. Lett.* 256, 389–402.
- Mabesoone, J.M., 1965. Composition and origin of 'Pedra Canga' and related ironstones in north-eastern Brazil. *Geol. Mijnb.* 44, 231–241.
- Machado, N., Lindenmayer, Z., Krogh, T.E., Lindenmayer, D., 1991. U-Pb geochronology of Archean magmatism and basement reactivation in the Carajás area, Amazon shield, Brazil. *Precambrian Res.* 49, 329–354.
- Margerison, H.R., Phillips, W.M., Stuart, F.M., Sudgen, D.E., 2005. Cosmogenic ^3He concentrations in ancient flood deposits from the Coombs Hills, northern Dry Valleys, East Antarctica: interpreting exposure ages and erosion rates. *Earth Planet. Sci. Lett.* 230, 163–175.
- Masarik, J., 2002. Numerical simulation of in-situ production of cosmogenic nuclides. *Geochim. Cosmochim. Acta* 66, A491.
- Masarik, J., Reedy, R.C., 1995. Terrestrial cosmogenic-nuclide production systematics calculated from numerical simulations. *Earth Planet. Sci. Lett.* 136, 381–395.
- Merrihue, C., 1964. Rare gas evidence for cosmic dust in modern Pacific red clay. *Ann. N. Y. Acad. Sci.* 119, 351–367.
- Meybeck, M., 1987. Global chemical weathering of surficial rocks estimated from river dissolved loads. *Am. J. Sci.* 287, 401.
- Monteiro, H.S., 2011. Geocronologia de Intemperismo por (U-Th)/He em Goethitas e Hematas Supergênicas das Canchas do Quadrilátero Ferrífero, Minas Gerais, Brasil. Instituto de Geociências, da Universidade Federal do Rio de Janeiro.
- Mukhopadhyay, S., Farley, K.A., 2006. New insights into the carrier phase(s) of extraterrestrial ^3He in geologically old sediments. *Geochim. Cosmochim. Acta* 70, 5061–5073.
- Niedermann, S., Graf, T., Marti, K., 1993. Mass-spectrometric identification of cosmic-ray-produced neon in terrestrial rocks with multiple neon components. *Earth Planet. Sci. Lett.* 118, 65–73.
- Ozima, M., Takayanagi, M., Zashu, S., Amari, S., 1984. High ^3He / ^4He ratios in ocean sediments. *Nature* 311, 449–451.
- Ramanaidou, E.R., 2009. Genesis of lateritic iron ore from banded iron-formation in the Capanema mine (Minas Gerais, Brazil). *Aust. J. Earth Sci.* 56, 605–620.
- Rood, D.H., Hall, S., Guilderson, T.P., Finkel, R.C., Brown, T.A., 2010. Challenges and opportunities in high-precision ^{10}Be – ^{10}Al measurements at CAMS. *Nucl. Instrum. Methods Phys. Res., Sect. B* 268, 730–732.
- Samama, J.C., 1986. Ore Fields and Continental Weathering. Van Nostrand Reinhold, New York.
- Schafer, J.M., Ivy-Ochs, S., Wieler, R., Leya, J., Baur, H., Denton, G.H., Schlüchter, C., 1999. Cosmogenic noble gas studies in the oldest landscape on earth: surface exposure ages of the Dry Valleys, Antarctica. *Earth Planet. Sci. Lett.* 167, 215–226.
- Shuster, D.L., Vasconcelos, P.M., Heim, J.A., Farley, K.A., 2005. Weathering geochronology by (U-Th)/He dating of goethite. *Geochim. Cosmochim. Acta* 69, 659–673.
- Shuster, D.L., Balco, G., Cassata, W.S., Fernandes, V.A., Garrick-Bethell, I., Weiss, B.P., 2010. A record of impacts preserved in the lunar regolith. *Earth Planet. Sci. Lett.* 290, 155–165.
- Spier, C.A., de Oliveira, S., Sial, A.N., Rios, F.J., 2007. Geochemistry and genesis of the banded iron formations of the Cau Formation, Quadrilátero Ferrífero, Minas Gerais, Brazil. *Precambrian Res.* 152, 170–206.
- Stone, J.O., 2000. Air pressure and cosmogenic isotope production. *J. Geophys. Res.* 105, 23753–23759.
- Stone, J.O., 2004. Extraction of Al and Be from quartz for isotopic analysis. University of Washington Cosmogenic Nuclide Lab Methods and Procedures. Online: <http://depts.washington.edu/cosmolab/chem.html>.
- Stone, J.O.H., Evans, J.M., Fifield, L.K., Allan, G.L., Cresswell, R.G., 1998. Cosmogenic chlorine-36 production in calcite by muons. *Geochim. Cosmochim. Acta* 62, 433–454.
- Teixeira, J.B.G., Eggler, D.H., 1994. Petrology, geochemistry, and tectonic setting of Archean basaltic and dioritic rocks from the N4 iron deposit, Serra dos Carajás, Pará, Brazil. *Acta Geol. Leopoldensia* 17, 71–114.
- Trendall, A.F., Basei, M.A.S., De Laeter, J.R., Nelson, D.R., 1998. SHRIMP zircon U-Pb constraints on the age of the Carajás formation, Grão Pará Group, Amazon Craton. *J. South Amer. Earth Sci.* 11, 265–277.
- Vasconcelos, P.M., 1999. K-Ar and ^{40}Ar / ^{39}Ar geochronology of weathering processes. *Annu. Rev. Earth Planetary Sci.* 27, 183–229.
- Vasconcelos, P.M., 2008. Re-weathering of Deep Weathering Profiles. International Geological Congress, Oslo.
- Vasconcelos, P.M., Conroy, M., 2003. Geochronology of weathering and landscape evolution, Dugald River valley, NW Queensland, Australia. *Geochim. Cosmochim. Acta* 67, 2913–2930.
- Vasconcelos, P.M., Becker, T.A., Renne, P.R., Brimhall, G.H., 1992. Age and duration of weathering by ^{40}K – ^{40}Ar and ^{40}Ar / ^{39}Ar analysis of potassium–manganese oxides. *Science* 258, 451.
- Vasconcelos, P.M., Brimhall, G.H., Becker, T.A., Renne, P.R., 1994a. ^{40}Ar / ^{39}Ar analysis of supergene jarosite and alunite; implications to the paleoweathering history of the Western USA and West Africa. *Geochim. Cosmochim. Acta* 58, 401–420.
- Vasconcelos, P.M., Renne, P.R., Brimhall, G.H., Becker, T.A., 1994b. Direct dating of weathering phenomena by ^{40}Ar / ^{39}Ar and K-Ar analysis of supergene K-Mn oxides. *Geochim. Cosmochim. Acta* 58, 1635–1665.
- Vasconcelos, P.M., Knesel, K.M., Cohen, B.E., Heim, J.A., 2008. Geochronology of the Australian Cenozoic: a history of tectonic and igneous activity, weathering, erosion, and sedimentation*. *Aust. J. Earth Sci.* 55 (6), 865–914.
- Yapp, C.J., Shuster, D.L., 2011. Environmental memory and a possible seasonal bias in the stable isotope composition of (U-Th)/He-dated goethite from the Canadian Arctic. *Geochim. Cosmochim. Acta* 75, 4194–4215.